代表文章 3

OH 自由基参与的反应被认为是多氯代二噁英(PCDD/Fs)在大气中的主要消除过程。我们采用密度泛函理论和正则变分过渡态理论研究了 OH 自由基引发的 2,3,7,8-TCDF 大气化学反应过程与动力学。TCDF 与 OH 自由的反应机理以及随后的反应过程包括呋喃环的键断裂，O_2 的加成或抽提，脱氯过程，过氧自由基 TCDF-OH-O_2 与 NO 的双分子的反应,羰基自由基 TCDF-OH-O 与 H_2O 的反应。在 TCDF-OH 的后续反应中，O_2 抽提与脱氯过程为主要反应路径。得到的产物中，HO_2 自由基和 Cl 原子活性较强，在整个大气氧化过程起到了重要的作用。最后，我们计算了 TCDF 与 OH 自由基反应的速率常数，与之前报道的实验数据一致。

Environmental Science & Technology

Article

pubs.acs.org/est

Atmospheric Chemical Reactions of 2,3,7,8-Tetrachlorinated Dibenzofuran Initiated by an OH Radical: Mechanism and Kinetics Study

Xiaomin Sun,[†,‡] Chenxi Zhang,[†] Yuyang Zhao,[†] Jing Bai,[†] Qingzhu Zhang,*[,†] and Wenxing Wang[†]

[†]Environment Research Institute, Shandong University, Jinan 250100, P. R. China

[‡]State Key Laboratory of Solid Lubrication, Lanzhou Institute of Chemical Physics, Chinese Academy of Science, Lanzhou 730000, P. R. China

Supporting Information

ABSTRACT: Reactions with the OH radical are expected to be the dominant removal processes for gas-phase polychlorinated dibenzo-*p*-dioxins and dibenzofuran (PCDD/Fs). The OH-initiated atmospheric chemical reaction mechanism and kinetics of 2,3,7,8-tetrachlorinated dibenzofuran (TCDF) are researched using the density functional theory and canonical variational transition state theory. The reaction mechanism of TCDF with the OH radical and ensuing reactions including bond cleavage of furan ring, O_2 addition or abstraction, dechlorination process, bimolecular reaction of TCDF-OH-O_2 peroxy radical with NO, and reaction of carbonyl free radicals TCDF-OH-O with H_2O are investigated. In the subsequent reactions of TCDF-OH, O_2 abstraction and dechlorination are most likely to predominate the process. As the main products, the HO_2 radical and the Cl atom are active and may play important roles in the atmospheric oxidation processes. The rate constants of TCDF with the OH radical are calculated, which are consistent with the reported data.

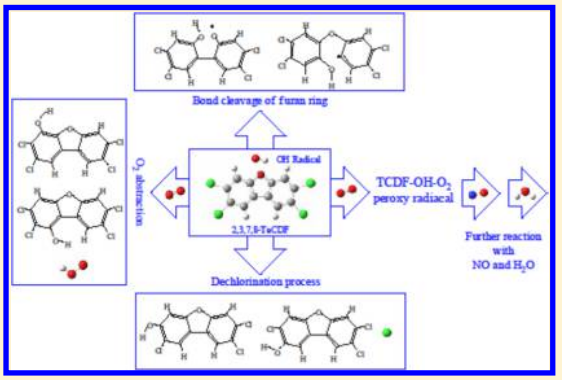

1. INTRODUCTION

Incineration has been considered the most effective strategy to dispose of toxic and infectious components in medical and municipal solid waste.[1−4] Among emissions from incineration processes, persistent organic pollutants (POPs), which mainly include polycyclic aromatic hydrocarbons (PAHs), polychlorinated biphenyls (PCBs), and polychlorinated dibenzo-*p*-dioxins and dibenzofurans (PCDD/Fs), are of scientists' concern due to their properties of persistence and bioaccumulation. PAHs are present at high levels in the incineration gas emissions, while PCDD/Fs often appear at much lower concentrations.[5] However, PCDD/Fs are some of the most important pollutants to be researched in stack emissions from incineration processes since they have carcinogenic, teratogenic, and mutagenic effects.

Many studies have focused on PCDD/Fs concentration, transformation, and transport in atmosphere.[6−10] The dominant removal processes of PCDD/Fs in the troposphere are wet and dry deposition, photolysis reaction, and chemical reaction with OH, HO_2, NO_3 radicals, and O_3.[11] The OH-initiated reactions are expected to play a major role in the atmospheric chemistry of PCDD/Fs.[12−14] It is necessary to study the mechanism and kinetics of the atmospheric chemical reactions in order to understand the atmospheric behavior of PCDD/Fs.

It is worth noting that subsequent reactions will occur easily in the atmosphere after the OH-initiated reactions of PCDD/Fs. Our previous work involved the OH-initiated atmospheric oxidation reaction of 2,3,7,8-tetrachlorinated dibenzo-p-dioxin (2,3,7,8-TeCDD).[15] This study can serve as a template for subsequent atmospheric degradation of the gaseous PCDD congeners. The reaction mechanisms of PCDFs presented by Altarawneh are drastically different from the atmospheric oxidations of PCDDs.[16] However, these reaction processes are incomplete, and only the reaction of O_2 with DF-OH(1) adduct is considered, though other adducts also account for a significant proportion. According to the electrophilic aromatic substitution mechanism, dibenzofuran (DF) in fly ash of waste incinerators can be converted to PCDFs in a N_2/O_2/HCl atmosphere, especially 2,3,7,8-substituted congeners.[17,18] Thus, 2,3,7,8-tetrachlorinated dibenzofuran (2,3,7,8-TeCDF, the following abbreviation is TCDF) was chosen to perform a comprehensive computational study.

Theoretical study can provide accurate predictions for the reaction mechanism through calculating the energetics and can offer kinetic data for key elementary reactions.[19−21] In this paper, density functional theory (DFT) is used to investigate the reaction mechanism of TCDF with the OH radical and the

Received: April 9, 2012
Revised: July 6, 2012
Accepted: July 11, 2012
Published: July 12, 2012

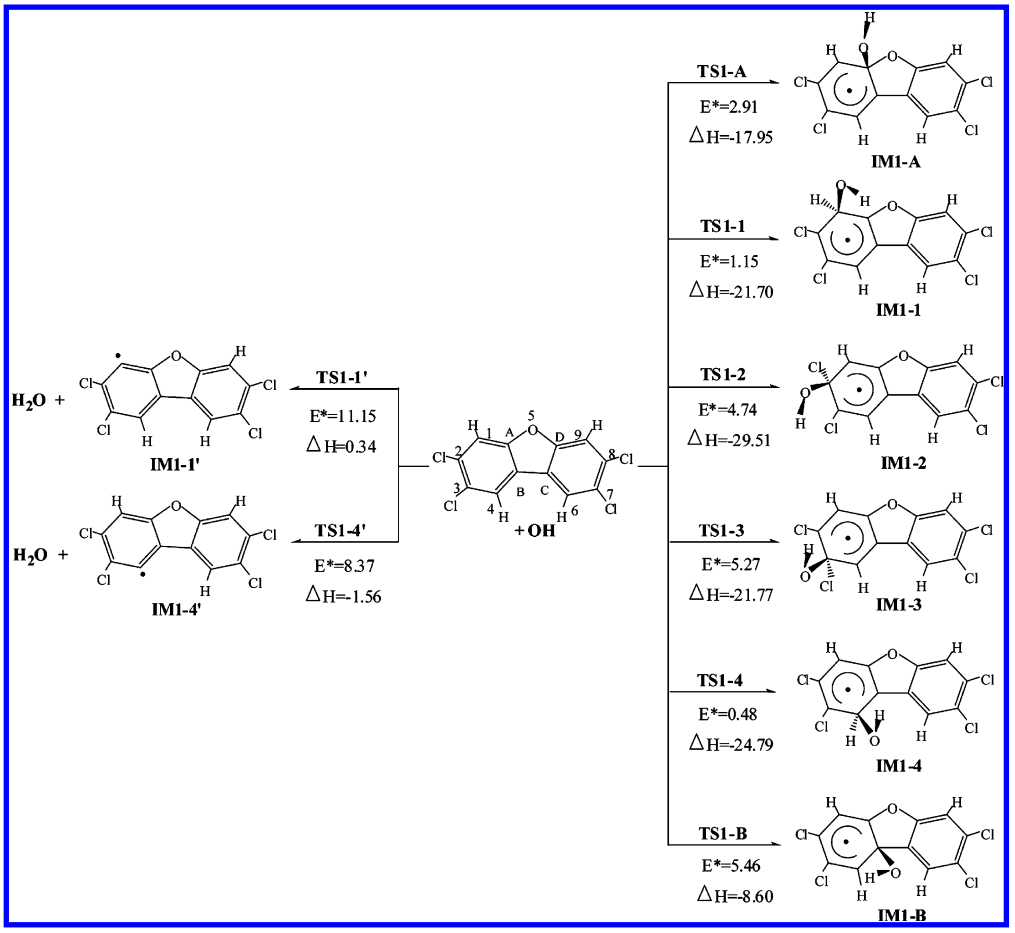

Figure 1. Possible pathways for the reactions of TCDF and the OH radical with the potential barriers E* (kcal/mol) and reaction heats ΔH (kcal/mol) at the MPWB1K/MG3S//MPWB1K/6-31+G(d,p) level.

ensuing reactions, such as bond cleavage of the furan ring, O_2 addition or abstraction, dechlorination process, and bimolecular reactions of TCDF-OH-O_2 peroxy radicals with NO. On the basis of the quantum chemical information, the rate constants are calculated using canonical variational transition state theory (CVT)[22,23] with small-curvature tunneling (SCT)[24] over a temperature range of 200—400 K.

2. COMPUTATIONAL METHODS

Structure optimizations of reactants, transition states, intermediates, and products were calculated using the MPWB1K method with the 6-31+G(d,p) basis set. MPWB1K is one of the best DFT methods for calculating barrier heights and reaction energies relative to computational cost.[25] All open-shell species were treated with an unrestricted approach, while closed-shell species were described with a restricted method. Structure optimizations were performed in Cartesian coordinates with an energy convergence criterion of 10^{-7} Hartree. Vibrational frequencies, calculated at the same level, were scaled by a standard scaling factor of 0.9335 to remove systematic error (provide a better estimate of the zero-point energy).[26] Each transition state was verified to connect the designated reactants and products by performing an intrinsic reaction coordinate (IRC) analysis.[27] The $<S^2>$ eigenvalues are in the range of 0.751−0.802 for doublet species and 2.013 for triplet species. Since the values of the total spin do not exceed an uncertainty of more than 10%, the spin contamination is not considered to be severe. As the rate constant calculations are sensitive to the activation energy, the single-point calculations have been performed with the MG3S basis sets, which is identical to 6-311+G(2df,2p) for H, C, and O elements, and very similar to 6-311+G(3d2f) for Cl element.[28] Zheng and Truhlar tested the performance of MPWB1K/MG3S on the calculation of barrier heights. The mean unsigned error for the barrier heights is 1.24 kcal/mol, which approximates the "chemical accuracy" goal of 1 kcal/mol.[29] All the calculations were performed using the Gaussian 03 programs.[30]

The CVT with SCT contribution is an effective method to calculate the rate constants.[31,32] In this paper, this method is used to calculate the rate constants of the elementary reaction over a suitable temperature range. All the dynamic calculations were carried out using the POLYRATE 9.7 program.[33]

3. RESULTS AND DISCUSSION

3.1. OH-Initiated Reaction. Under the atmospheric conditions, the chemical reactions of TCDF are initiated easily by the OH radical. Two possible reaction patterns are taken into consideration, i.e., OH radical addition and H atom abstraction. The probable pathways for the reactions of TCDF with the OH radical are depicted in Figure 1, in which the potential barriers (E*) and the reaction heats (ΔH) calculated at the MPWB1K/MG3S//MPWB1K/6-31+G(d,p) level are also given.

3.1.1. OH Radical Addition Pathways. Because of its C_2 symmetry, TCDF has six different addition positions, that is, the four different carbon atoms in the benzene ring (C_1—C_4),

dx.doi.org/10.1021/es301413v | Environ. Sci. Technol. 2012, 46, 8148−8155

Table 1. Rate Constants k (cm^3 $molecule^{-1}$ s^{-1}) and Branching Ratios R at 298.15 K and Arrhenius Formulas for Initial Reactions over the Temperature Range of 200−400 K[a]

reactions	$k_{298.15K}$	R	Arrhenius formulas
TCDF + OH → IM1-A	7.14×10^{-14}	0.07	$k(T) = 1.10 \times 10^{-11}\left(\frac{T}{300}\right)^{2.08} \exp(-12451.63/RT)$
TCDF + OH → IM1-1	1.90×10^{-13}	0.19	$k(T) = 2.86 \times 10^{-12}\left(\frac{T}{300}\right)^{2.07} \exp(-6689.94/RT)$
TCDF + OH → IM1-2	4.03×10^{-15}	4.12×10^{-3}	$k(T) = 1.71 \times 10^{-11}\left(\frac{T}{300}\right)^{1.90} \exp(-20675.92/RT)$
TCDF + OH → IM1-3	1.08×10^{-15}	1.10×10^{-3}	$k(T) = 6.68 \times 10^{-12}\left(\frac{T}{300}\right)^{2.57} \exp(-21605.01/RT)$
TCDF + OH → IM1-4	7.07×10^{-13}	0.72	$k(T) = 2.05 \times 10^{-12}\left(\frac{T}{300}\right)^{2.21} \exp(-2603.11/RT)$
TCDF + OH → IM1-B	9.75×10^{-16}	9.97×10^{-4}	$k(T) = 8.19 \times 10^{-12}\left(\frac{T}{300}\right)^{2.27} \exp(-22363.83/RT)$
TCDF + OH → IM1-1′ + H_2O	2.33×10^{-17}	2.38×10^{-5}	$k(T) = 5.79 \times 10^{-14}\left(\frac{T}{300}\right)^{2.79} \exp(-19337.20/RT)$
TCDF + OH → IM1-4′ + H_2O	2.60×10^{-15}	2.67×10^{-3}	$k(T) = 7.95 \times 10^{-14}\left(\frac{T}{300}\right)^{2.51} \exp(-8431.64/RT)$

[a]Calculated at the MPWB1K/MG3S//MPWB1K/6-31+G(d,p) level. Total addition: 9.75×10^{-13}, total abstraction: 2.63×10^{-15}, overall: 9.78×10^{-13}, overall (ref 11): $(0.40-1.00) \times 10^{-12}$.

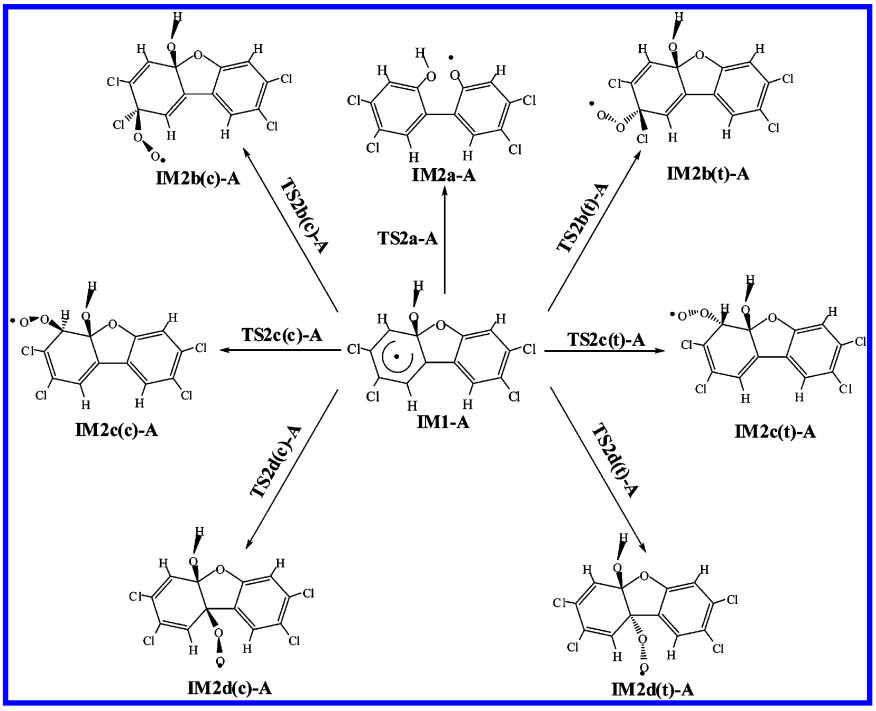

Figure 2. Possible pathways for the subsequent reactions of IM1-A.

the oxygen-bonded carbon in the furan ring (C_A), and the carbon-bonded carbon in the furan ring (C_B). The rate constants (k) and branching ratios (R) at 298.15 K of the elementary reactions are listed in Table 1, and after the errors were considered, the rate constants at 298.15 K are listed in Table S1. From Figure 1 and Table 1, it is easy to see that the C_1-addition and C_4-addition are both thermodynamically and kinetically favorable since the barriers are low (1.15 and 0.48 kcal/mol, respectively), and the rate constants are large (1.90×10^{-13} cm^3 $molecule^{-1}$ s^{-1} and 7.07×10^{-13} cm^3 $molecule^{-1}$ s^{-1}, respectively). As indicated by the E* values and the ΔH values, all the barriers to OH radical addition reactions are no more than 5.50 kcal/mol, and the reactions are strongly exothermic (ΔH←8.60 kcal/mol). Thus every OH addition reaction can occur easily. In general, the branching ratios R of C_4-addition will decrease as the temperature rises, while the branching ratios R of C_A-addition and C_1-addition increase noticeably, and the branching ratios R of other addition reactions are elevated slightly (Figure S1). Different addition positions play a varied

Table 2. Potential Barriers E* (kcal/mol), the Reaction Heats ΔH (kcal/mol), and the Rate Constants k (Units are s^{-1} and cm^3 $molecule^{-1}$ s^{-1} for Unimolecular and Bimolecular Reactions, Respectively) at 298.15 K[a]

reactions	E*	ΔH	$k_{298.15K}$	reactions	E*	ΔH	$k_{298.15K}$
IM1-A → IM2a-A	21.86	−7.47	1.48×10^{-2}	IM1-3 → IM2a-3 + Cl	1.28	−2.76	5.01×10^{11}
IM1-A + O_2 → IM2b(c)-A	12.52	−1.41	4.91×10^{-25}	IM1-3 + O_2 → IM2b(c)-3	7.53	−1.06	1.69×10^{-21}
IM1-A + O_2 → IM2c(c)-A	17.57	−7.83	1.83×10^{-28}	IM1-3 + O_2 → IM2c(c)-3	6.38	−14.94	8.23×10^{-21}
IM1-A + O_2 → IM2d(c)-A	15.71	−1.43	2.16×10^{-27}	IM1-3 + O_2 → IM2d(c)-3	9.46	0.28	5.83×10^{-23}
IM1-A + O_2 → IM2b(t)-A	13.47	−0.51	7.89×10^{-26}	IM1-3 + O_2 → IM2b(t)-3	8.84	−0.89	1.12×10^{-22}
IM1-A + O_2 → IM2c(t)-A	13.02	−7.69	1.37×10^{-25}	IM1-3 + O_2 → IM2c(t)-3	7.29	−9.08	3.12×10^{-21}
IM1-A + O_2 → IM2d(t)-A	15.36	8.99	4.15×10^{-27}	IM1-3 + O_2 → IM2d(t)-3	12.30	0.17	4.71×10^{-25}
IM1 − 1 + O_2 → IM2a − 1 + HO_2	15.31	−28.91	5.73×10^{-19}	IM1-4 + O_2 → IM2a-4 + HO_2	16.89	−26.13	8.96×10^{-19}
IM1-1 + O_2 → IM2b(c)-1	4.74	−9.72	9.74×10^{-20}	IM1-4 + O_2 → IM2b(c)-4	5.29	−6.07	5.17×10^{-20}
IM1-1 + O_2 → IM2c(c)-1	8.61	−3.87	3.56×10^{-22}	IM1-4 + O_2 → IM2c(c)-4	9.36	−3.63	5.85×10^{-23}
IM1-1 + O_2 → IM2d(c)-1	9.25	−2.11	8.81×10^{-23}	IM1-4 + O_2 → IM2d(c)-4	14.16	6.25	2.03×10^{-26}
IM1 − 1 + O_2 → IM2b(t)-1	6.88	−8.14	3.53×10^{-21}	IM1-4 + O_2 → IM2b(t)-4	7.54	−5.34	2.86×10^{-21}
IM1-1 + O_2 → IM2c(t)-1	9.15	−3.84	7.17×10^{-23}	IM1-4 + O_2 → IM2c(t)-4	9.73	−3.23	3.72×10^{-23}
IM1 − 1 + O_2 → IM2d(t)-1	9.36	−1.71	5.12×10^{-23}	IM1-4 + O_2 → IM2d(t)-4	14.54	6.78	1.07×10^{-26}
IM1-2 → IM2a − 2 + Cl	1.18	−1.15	7.53×10^{11}	IM1-B → IM2a-B	38.82	23.74	6.24×10^{-13}
IM1-2 + O_2 → IM2b(c)-2	14.23	10.81	3.34×10^{-26}	IM1-B + O_2 → IM2b(c)-B	8.37	−6.63	4.88×10^{-22}
IM1-2 + O_2 → IM2c(c)-2	12.48	3.58	4.13×10^{-25}	IM1-B + O_2 → IM2c(c)-B	16.96	−7.67	3.12×10^{-28}
IM1 − 2 + O_2 → IM2d(c)-2	10.57	−5.57	9.25×10^{-24}	IM1-B + O_2 → IM2d(c)-B	11.25	−10.18	2.78×10^{-24}
IM1-2 + O_2 → IM2b(t)-2	16.18	9.49	6.12×10^{-28}	IM1-B + O_2 → IM2b(t)-B	9.31	−3.91	6.85×10^{-23}
IM1-2 + O_2 → IM2c(t)-2	18.13	6.38	4.37×10^{-29}	IM1-B + O_2 → IM2c(t)-B	15.12	−10.16	6.36×10^{-27}
IM1-2 + O_2 → IM2d(t)-2	15.83	−1.76	9.06×10^{-28}	IM1-B + O_2 → IM2d(t)-B	10.17	0.73	2.19×10^{-23}

[a]Calculated at the MPWB1K/MG3S//MPWB1K/6-31+G(d,p) level. The oxygen addition of IM1-A: 7.13×10^{-25}, the oxygen addition of IM1-1: 1.01×10^{-19}, the oxygen addition of IM1-2: 9.70×10^{-24}, the oxygen addition of IM1-3: 1.32×10^{-20}, the oxygen addition of IM1-4: 5.46×10^{-20}, the oxygen addition of IM1-B: 5.81×10^{-22}.

role as temperature changes. Therefore, further studies on all the OH addition reactions are necessary.

3.1.2. H Atom Abstraction Pathways. Due to its nucleophilicity, the OH radical can abstract the H atom from the benzene ring to form the dibenzofuranyl radical isomers (IM1-1′ and IM1-4′). The barriers are 11.15 and 8.37 kcal/mol, respectively, which are much higher than those of OH radical addition pathways. The reaction heats of the above two H atom abstraction pathways are 0.34 kcal/mol and −1.56 kcal/mol, which implies that the reactions are endothermic or slightly exothermic. In addition, the total abstraction rate constant is 2.63×10^{-15} cm^3 $molecule^{-1}$ s^{-1} (the sum of 2.33×10^{-17} cm^3 $molecule^{-1}$ s^{-1} and 2.60×10^{-15} cm^3 $molecule^{-1}$ s^{-1}). The branching ratios R for IM1-1′ and IM1-4′ at 298.15 K are only 2.38×10^{-5} and 2.67×10^{-3}, respectively. Hence, the H atom abstraction reaction is not dominant in contrast with the addition to the benzene ring, and it can be negligible in the following reaction.

3.1.3. The Atmospheric Lifetime τ. Under atmospheric conditions, OH-initiated reactions are probably the most important atmospheric removal pathways for PCDD/Fs. The atmospheric lifetime (τ) of TCDF can be approximated by $\tau = 1/(k_{OH}\,[OH])$, and here the average OH radical concentration [OH] is 9.7×10^5 molecules cm^{-3}.[34] Atkinson has determined that the rate constants of T_4CDF (PCDF with four Cl atoms) vary in the range of $0.40-1.00 \times 10^{-12}$ cm^3 $molecule^{-1}$ s^{-1} based on the structure−activity relationship (SAR) at room temperature, and the calculated tropospheric lifetimes relative to the OH radical were 11.93−29.83 days.[11] Sinkkonen also estimated that the half-life time of TCDF in air was 320 h, when the photodegradation is considered only due to the OH radical.[35] In other words, the lifetime of TCDF was 19.23 days.

Given the errors, the total rate constant for abstraction and addition at 298.15 K is $2.15 \times 10^{-13}-5.93 \times 10^{-12}$ cm^3 $molecule^{-1}$ s^{-1} (Table S1). At the MPWB1K/MG3S//MPWB1K/6-31+G(d,p) level, the total rate constant at 298.15 K is 9.78×10^{-13} cm^3 $molecule^{-1}$ s^{-1} and the atmospheric lifetime of TCDF is 12.20 days, which is relatively consistent with the value reported by Atkinson and Sinkkonen.[11,35]

3.2. Subsequent Reactions for the IM1 in Atmosphere. As highly activated open-shell species, further reactions of IM1 will occur in atmosphere, for example, decomposition, isomerization, or reaction with O_2 ($^3\sum_g$).

3.2.1. IM1-A and IM1-B. The probable pathways of IM1-A and IM1-B are clarified in Figure 2 and Figure S4. Meanwhile, the potential barrier E* and reaction heat ΔH calculated at the MPWB1K/MG3S//MPWB1K/6-31+G(d,p) level and rate constants k at 298.15 K are listed in Table 2. Because both IM1-A and IM1-B share the similar subsequent pathways, the former was selected as an example. After the addition of the OH radical to the C_A position, the adjacent C−O bond in the furan ring is elongated by 0.070 Å, compared to the corresponding bond in the TCDF. Then it can lead to the

dx.doi.org/10.1021/es301413v | Environ. Sci. Technol. 2012, 46, 8148−8155

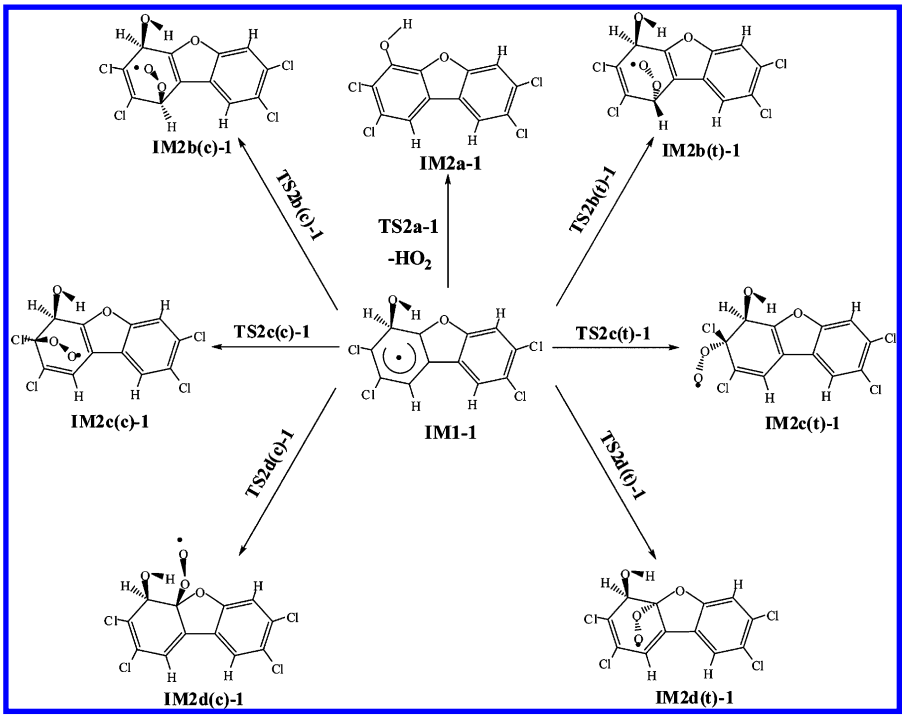

Figure 3. Possible pathways for the subsequent reactions of IM1-1.

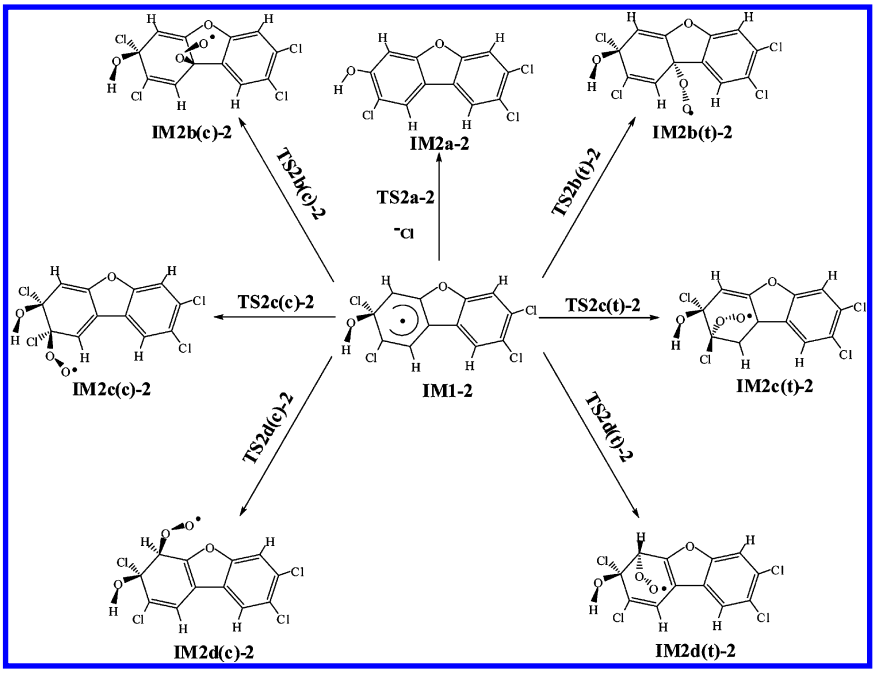

Figure 4. Possible pathways for the subsequent reactions of IM1-2.

breakup of the furan ring and formation of IM2a-A with a barrier of 21.86 kcal/mol. 7.47 kcal/mol of heat is released in the bond cleavage process, and the unimolecular rate constant is 1.48×10^{-2} s^{-1}.

Moreover, the O_2 can be added to the aromatic rings from the same or opposite side of the dioxin ring (*cis*-addition and the *trans*-addition) with respect to the OH group. The O_2 addition to the π-delocalized electron systems of the IM1-A adducts occurs on the two ortho-carbon atoms of the C_A position as well as to the para-carbon, producing peroxy radical isomers as depicted in Figure 2. The E* range of addition reactions varies from 12.52 to 17.57 kcal/mol, which is lower than those of the bond cleavage process. Furthermore, all the reactions are exothermic except the formation of IM2d(t)-A, giving out 8.99 kcal/mol of energy. The total rate constant for the oxygen addition of IM1-A is 7.13×10^{-25} cm^3 $molecule^{-1}$ s^{-1} (Table 2). Usually, the O_2 concentration in atmosphere is supposed to be a constant with the value of 4.92×10^{18} molecules cm^{-3}. Then the bimolecular reaction can be treated as a pseudofirst-order reaction, and the rate constant is 3.50×10^{-6} s^{-1}. The rate constant of oxygen addition is much lower

dx.doi.org/10.1021/es301413v | *Environ. Sci. Technol.* 2012, 46, 8148−8155

than that in the bond cleavage process. Thus, IM1-A is kinetically favored to open up the C−O bond.

It is worthwhile to note that the cleavage of C−C bond in IM1-B is impeded by a high potential barrier of 38.82 kcal/mol, and this process is strongly endothermic and releases 23.74 kcal/mol of energy. Furthermore, the rate constant of this unimolecular isomerization is 6.24×10^{-13} s^{-1} (Table 2), while the total rate constant of oxygen addition is 5.81×10^{-22} cm^3 $molecule^{-1}$ s^{-1} (Table 2), that is, the rate constant of the pseudofirst-order reaction is 2.86×10^{-4} s^{-1}. As a result, oxygen addition is important in IM1-B reactions.

3.2.2. IM1-1 and IM1-4. The oxygen addition pathways of IM1-1 and IM1-4, as displayed in Figure 3 and Figure S3, are similar to those of IM1-A and IM1-B. The O_2 can also be added to the aromatic ring, which will lead to the formation of peroxy radical isomers that can further react with NO. The total addition rate constants of IM1-1 and IM1-4 are 1.01×10^{-19} cm^3 $molecule^{-1}$ s^{-1} and 5.46×10^{-20} cm^3 $molecule^{-1}$ s^{-1} (Table 2), respectively.

Different from IM1-A and IM1-B, the subsequent reactions of IM1-1 and IM1-4 can produce the closed shell dibenzofuranol structures (IM2a-1 and IM2a-4) and HO_2 radical (Figure 3 and Figure S2). The barriers are 15.31 and 16.89 kcal/mol, and these processes are strongly exothermic and give out heat by up to 28.91 and 26.13 kcal/mol, respectively. The rate constant for abstraction reaction (5.73×10^{-19} cm^3 $molecule^{-1}$ s^{-1}, Table 2) of IM1-1 is about 5.67 times faster than that of oxygen addition reaction. Then the O_2 addition can possibly compete with the formation of IM2a-1 and HO_2 radical. The rate constant (8.96×10^{-19} cm^3 $molecule^{-1}$ s^{-1}, Table 2) in the formation of IM2a-4 and HO_2 radical is much higher than the total addition rate constants of IM1-4. Hence, IM1-4 is most likely to transform to IM2a-4 and the HO_2 radical. The HO_2 radical, with a very short photochemical lifetime, is quite active and plays important roles in the atmospheric oxidation processes.[36]

3.2.3. IM1-2 and IM1-3. The distinction between the further reaction of IM1-2 and IM1-3 (Figure 4 and Figure S2) and other OH adducts can be found in the dechlorination process. In IM1-2 and IM1-3, the Cl atoms in the aromatic ring can be removed to generate two closed shell dibenzofuranol structures (IM2a-2 and IM2a-3). Rate constants for addition reactions of IM1-2 and IM1-3 are 4.77×10^{-5} s^{-1} and 6.49×10^{-2} s^{-1} after converting to the pseudofirst-order rate constant. These dechlorination reactions are the dominant pathway since their barriers are low (1.18 and 1.28 kcal/mol) and the rate constants are large (7.53×10^{11} s^{-1} and 5.01×10^{11} s^{-1}, Table 2).

The product, Cl atom, is a highly active radical which can play a significant role in the oxidative chemistry of the troposphere. The Cl atom has faster rate constants than those of the OH radical with methane and nonmethane hydrocarbons, which may play an important role in controlling the lifetime of important greenhouse gases.[37] In addition, the Cl atom can intensify the ozone depletion.[38] Then the OH-initiated dechlorination process of TCDF will affect the environment and human health negatively.

3.3. Reactions of TCDF-OH-O_2 Peroxy Radical in Atmosphere. With regard to the TCDF-OH-O_2 peroxy radical isomers, they can be cyclized when the O atom of oxygen attacks the C atoms of the furan ring or the benzene ring. In the similar reactions of TCDD-OH-O_2, the ring closure process must overcome a large barrier (18.0−24.9 kcal/mol), while the reaction of the TCDD-OH-O_2 peroxy radical with NO is a barrierless association.[15] Therefore, the reaction with NO in atmosphere is the main removal way of the peroxy radical isomers. According to the E* and rate constants, the most plausible TCDF-OH-O_2 adduct IM2b(c)-B is affirmed in this study (calculated at the MPWB1K/MG3S//MPWB1K/6-31+G(d,p) level). This reaction is strongly endothermic, releasing 17.69 kcal/mol of energy.

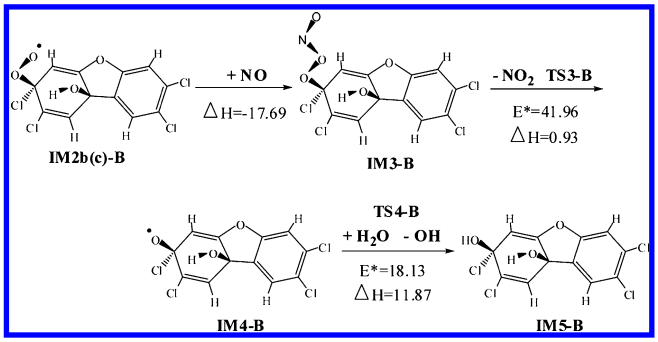

In the troposphere, the reaction of $RO_2 + NO \rightarrow RONO_2$ is a radical chain terminating step that can suppress ozone production. Thus, the TCDF-OH-O_2 peroxy radical can be regarded as a good depressor of photochemical smog. After overcoming the high barrier of 41.96 kcal/mol, TCDF-OH-ONO_2 (IM3-B) will result in the formation of carbonyl free radicals IM4-B. It is known that H_2O is the third most prevalent constituent, accounting for about 1.5% as vapor and about 2% if clouds and ice crystals are included. The H_2O reaction can not be ignored. The carbonyl free radicals IM4-B can abstract the H atom from H_2O to reach a stable state and the OH radical will be regenerated simultaneously. As the main chemical species affect the oxidizing capacity of the troposphere, the OH radical will initiate a new round of chemical reactions.

4. ENVIRONMENTAL SIGNIFICANCE

The atmospheric chemical reactions of TCDF initiated by ·OH have been researched. Two types of mechanisms including hydroxyl addition and hydrogen abstraction are considered. In the atmosphere, the chemical reactions of TCDF are initiated mainly by OH addition, while hydrogen abstraction takes up a tiny proportion. The atmospheric lifetime of TCDF is about 12.20 days, which is consistent with the previous report. In the subsequent reactions of IM1, IM1-A is kinetically favored to open up the C−O bond, while oxygen addition is more important for IM1-B; IM1-1 and IM1-4 are more likely to generate the closed shell dibenzofuranol structures and HO_2 radical. The dechlorinate processes of IM1-2 and IM1-3 are the dominant pathway. The HO_2 radical and Cl atom may play an important role in oxidative chemistry of troposphere. The reaction with atmospheric NO is the main fate of the peroxy radical isomers. Oxyl radicals are formed in the reactions of these isomers with the atmospheric NO. Then, H_2O molecule may act as an activator of the OH transfer, which quickens the chemistry process. This study can serve as a template for atmospheric degradation of the gaseous PCDF congeners, which is helpful in assessing their atmospheric behaviors.

■ ASSOCIATED CONTENT

Supporting Information

Figures S1−S5 and Tables S1 and S2. This material is available free of charge via the Internet at http://pubs.acs.org.

AUTHOR INFORMATION

Corresponding Author

*Fax: 86-531-8836 1990. E-mail: zqz@sdu.edu.cn (Q.Z.).

Notes

The authors declare no competing financial interest.

ACKNOWLEDGMENTS

This work was supported financially by the National Nature Science Foundation of China (No. 20977059, 20903062), National High Technology Research and Development Program 863 Project (2012AA06A301), Independent Innovation Foundation of Shandong University (IIFSDU, 2010TS064), and Open Project from State Key Laboratory of Environmental Chemistry and Ecotoxicology, Research Center for Eco-Environmental Sciences, Chinese Academy of Sciences (No. KF2009-10). Excellent young scientists award fund of Shandong Province (BS2012HZ009).

REFERENCES

(1) Chen, C. K.; Lin, C.; Lin, Y. C.; Wang, L. C.; Chang-Chien, G. P. Polychlorinated dibenzo-p-dioxins/dibenzofuran mass distribution in both start-up and normal condition in the whole municipal solid waste incinerator. *J. Hazard. Mater.* **2008**, *160* (1), 37−44.

(2) Hoyos, A.; Cobo, M.; Aristizábal, B.; Córdoba, F.; Montes de Correa, C. Total suspended particulate (TSP), polychlorinated dibenzodioxin (PCDD) and polychlorinated dibenzofuran (PCDF) emissions from medical waste incinerators in Antioquia, Colombia. *Chemosphere* **2008**, *73* (1), S137−S142.

(3) Hjelmar, O. Disposal strategies for municipal solid waste incineration residues. *J. Hazard. Mater.* **1996**, *47* (1−3), 345−368.

(4) Lee, C. C.; Huffman, G. L. Medical waste management/incineration. *J. Hazard. Mater.* **1996**, *35* (1−3), 3495−3501.

(5) Rivera-Austrui, J.; Borrajo, M. A.; Martinez, K.; Adrados, M. A.; Abalos, M.; Van Bavel, B.; Rivera, J.; Abad, E. Assessment of polychlorinated dibenzo-p-dioxin and dibenzofuran emissions from a hazardous waste incineration plant using long-term sampling equipment. *Chemosphere* **2011**, *82* (9), 1343−1349.

(6) Countinho, M.; Pereira, M.; Borrego, C. Monitoring of ambient air PCDD/F levels in Portugal. *Chemosphere* **2007**, *67* (9), 1715−1721.

(7) Armitage, J. M.; McLachlan, M. S.; Wiberg, K.; Jonsson, P. A model assessment of polychlorinated dibenzo-p-dioxin and dibenzofuran sources and fate in the Baltic Sea. *Sci. Total Environ.* **2009**, *407* (12), 3784−3792.

(8) Venier, M.; Ferrario, J.; Hites, R. A. Polychlorinated dibenzo-p-dioxins and dibenzofurans in the atmosphere around the great lakes. *Environ. Sci. Technol.* **2009**, *43* (4), 1036−1041.

(9) Li, Y. M.; Wang, T.; Wang, P.; Ding, L.; Li, X. M.; Wang, Y. W.; Zhang, Q. H.; Li, A.; Jiang, G. B. Reduction of atmospheric polychlorinated dibenzo-p-dioxins and dibenzofurans (PCDD/Fs) during the 2008 Beijing Olympic Games. *Environ. Sci. Technol.* **2011**, *45* (8), 3304−3309.

(10) Zhao, B.; Zheng, M. H.; Jiang, G. B. Dioxin emissions and human exposure in China: a brief history of policy and research. *Environ. Health Perspect.* **2011**, *119* (3), A112−A113.

(11) Atkinson, R. Atmospheric chemistry of PCBs, PCDDs and PCDFs. In *Issues in Environmental Science and Technology*; Hester, R. E., Harrison, R. M., Eds.; The Royal Society of Chemistry: Cambridge, U.K., 1996; Vol. *6*, pp 53−72.

(12) Baker, J. I.; Hites, R. A. Is combustion the major source of polychlorinated dibenzo-p-dioxins and dibenzofurans to the environment? A mass balance investigation. *Environ. Sci. Technol.* **2000**, *34* (14), 2879−2886.

(13) Brubaker, W. W.; Hites, R. A. Polychlorinated Dibenzo-p-dioxins and dibenzo-furans: gas-phase hydroxyl radical reactions and related atmospheric removal. *Environ. Sci. Technol.* **1997**, *31*, 1805−1810.

(14) Taylor, P. H.; Yamada, T.; Neuforth, A. Kinetics of OH radical reactions with dibenzo-p-dioxin and selected chlorinated dibenzo-p-dioxins. *Chemosphere* **2005**, *58*, 243−252.

(15) Zhang, C. X.; Sun, T. L.; Sun., X. M. Mechanism for OH-initiated degradation of 2,3,7,8-tetrachlorinated dibenzo-p-dioxins in the presence of O_2 and NO/H_2O. *Environ. Sci. Technol.* **2011**, *45*, 4756−4762.

(16) Altarawneh, M.; Kennedy, E. M.; Dlugogorski, B. Z.; Mackie, J. C. Computational Study of the Oxidation and Decomposition of Dibenzofuran under Atmospheric Conditions. *J. Phys. Chem. A* **2008**, *112* (30), 6960−6967.

(17) Addink, R.; Antonioli, M.; Olie, K.; Govers, H. A. J. Reactions of dibenzofuran and 1,2,3,4,7,8-hexachlorodibenzo-p-dioxin on municipal waste incinerator fly ash. *Environ. Sci. Technol.* **1996**, *30* (3), 833−836.

(18) Ryu, J. Y.; Choi, K. C.; Mulholland, J. A. Polychlorinated dibenzo-p-dioxin (PCDD) and dibenzofurna (PCDF) isomer patterns from municipal waste combustion: Formation mechanism fingerprints. *Chemosphere* **2006**, *65* (9), 1526−1536.

(19) Altarawneh, M.; Dlugogorski, B. Z.; Kennedy, E. M.; Mackie, J. C. Quantum Chemical Study of Low Temperature Oxidation Mechanism of Dibenzofuran. *J. Phys. Chem. A* **2006**, *110* (50), 13560−13567.

(20) Zhang, Q. Z.; Qu, X. H.; Wang, W. X. Mechanism of OH-initiated atmospheric photooxidation of dichlorvos: a quantum mechanical study. *Environ. Sci. Technol.* **2007**, *41* (17), 6109−6116.

(21) Zhou, J.; Chen, J. W.; Liang, C. H.; Xie, Q.; Wang, Y. N.; Zhang, S. Y.; Qiao, X. L.; Li, X. H. Quantum chemical investigation on the mechanism and kinetics of PBDE photooxidation by·OH: a case study for BDE-15. *Environ. Sci. Technol.* **2011**, *45* (11), 4839−4845.

(22) Baldridge, M. S.; Gordon, R.; Steckler, R.; Truhlar, D. G. Ab initio reaction paths and direct dynamics calculations. *J. Phys. Chem.* **1989**, *93* (13), 5107−5119.

(23) Gonzalez-Lafont, A.; Truong, T. N.; Truhlar, D. G. Interpolated variational transition-state theory: Practical methods for estimating variational transition-state properties and tunneling contributions to chemical reaction rates from electronic structure calculations. *J. Chem. Phys.* **1991**, *95* (12), 8875−8894.

(24) Liu, Y. P.; Lynch, G. C.; Truong, T. N.; Lu, D. H.; Truhlar, D. G.; Garrett, B. C. Molecular modeling of the kinetic isotope effect for the (1,5)-sigmatropic rearrangement of cis-1,3-pentadiene. *J. Am. Chem. Soc.* **1993**, *115* (6), 2408−2415.

(25) Zhao, Y.; Truhlar, D. G. Hybrid meta density functional theory methods for thermochemistry, thermochemical kinetics, and noncovalent interactions: the MPW1B95 and MPWB1K models and comparative assessments for hydrogen bonding and van der waals interactions. *J. Phys. Chem. A* **2004**, *108* (33), 6908−6918.

(26) Merrick, J. P.; Moran, D.; Radom, L. An evaluation of harmonic vibrational frequency scale factors. *J. Phys. Chem. A* **2007**, *111* (45), 11683−11700.

(27) Fukui, K. The path of chemical reactions-the IRC approach. *Acc. Chem. Res.* **1981**, *14* (12), 363−368.

(28) Lynch, B. J.; Zhao, Y.; Truhlar, D. G. Effectiveness of diffuse basis functions for calculating relative energies by density functional theory. *J. Phys. Chem. A* **2003**, *107* (9), 1384−1388.

(29) Zheng, J. J.; Zhao, Y.; Truhlar, D. G. The DBH24/08 database and its use to assess eectronic structure model chemistries for chemical reaction barrier heights. *J. Chem. Theory Comput.* **2009**, *5*, 808−821.

(30) Frisch, M. J.; Trucks, G. W.; Schlegel, H. B.; Pople, J. A. *Gaussian 03*, Revision E.01; Gaussian, Inc.: Pittsburgh PA, 2003.

(31) Garrett, B.; Truhlar, D. Variational transition-state theory. *Acc. Chem. Res.* **1980**, *13* (12), 440−448.

(32) Liu, Y. P.; Lynch, G. C.; Truong, T. N.; Lu, D. H.; Truhlar, D. G.; Garrett, B. C. Molecular modeling of the kinetic isotope effect for the [1,5]-sigmatropic rearrangement of cis-1,3-pentadiene. *J. Am. Chem. Soc.* **1993**, *115* (6), 2408−2415.

(33) Corchado, J. C.; Chuang, Y. Y.; Fast, P. L.; Villa, J.; Hu, W. P.; Liu, Y. P.; Lynch, G. C.; Nguyen, K. A.; Jackels, C. F.; Melissas, V. S.;

Lynch, B. J.; Rossi, I.; Coitino, E. L.; Ramos, A. F.; Pu, J.; Albu, T. V.; Garrett, R. B. C.; Truhlar, D. G. *POLYRATE version 9.7*; 2007.

(34) Prinn, R. G.; Weiss, R. F.; Miller, B. R.; Huang, J.; Alyea, F. N.; Cunnold, D. M.; Fraser, P. J.; Hartley, D. E.; Simmonds, P. G. Atmospheric trends and lifetime of CH_3CCl_3 and global OH concentrations. *Science* **1995**, *269*, 187−192.

(35) Sinkkonen, S.; Paasivirta, J. Degradation half-life times of PCDDs, PCDFs and PCBs for environmental fate modeling. *Chemosphere* **2000**, *40* (9−11), 943−949.

(36) Rena, X.; Harder, H.; Martinez, M.; Lesher, R. L.; Oliger, A.; Simpas, J. B.; Brune, W. H.; Schwab, J. J.; Demerjian, K. L.; Hed, Y.; Zhou, X. L.; Gao, H. L. OH and HO_2 Chemistry in the urban atmosphere of New York City. *Atmos. Environ.* **2003**, *37* (26), 3639−3651.

(37) Lawler1, M. J.; Sander, R.; Carpenter, L. J.; Lee, J. D.; Glasow, R.; Sommariva, R.; Saltzman, E. S. HOCl and Cl_2 observations in marine air. *Atmos. Chem. Phys.* **2011**, *11* (15), 7617−7628.

(38) Knipping, E. M.; Dabdub, D. Impact of chlorine emissions from sea-salt aerosol on coastal urban ozone. *Environ. Sci. Technol.* **2003**, *37* (2), 275−284.